Comparative Analysis of Bat Genomes Provides Insight into the Evolution of Flight and Immunity

Guojie Zhang *et al.*
Science **339**, 456 (2013);
DOI: 10.1126/science.1230835

giving the axonal cytoskeleton a long-range order. Despite the molecular composition differences between the axon initial segments and distal axons [for example, ankyrin-G and βIV-spectrin are confined in the axon initial segment by an exclusion effect of the distal axon proteins ankyrin-B and βII-spectrin (31)], the cytoskeletal organization is similar between the initial and distal segments of the axons, both adopting a quasi-1D, periodic structure. Interestingly, we found this periodic cytoskeleton structure to be present only in axons, not in dendrites, which instead primarily contained long actin filaments running along the dendritic axis. Although the microscopic interactions between the molecular components of the axon cytoskeleton are probably similar to those between the erythrocyte analogs (9, 10), the overall structure of this quasi-1D, periodic cytoskeleton in axons is distinct from the 2D, pentagonal or hexagonal structure observed for the erythrocyte membrane cytoskeleton (11, 12). In *Drosophila* motoneuron axons near the neuromuscular junctions, spectrin and ankyrin appear to organize into an erythrocyte-like, pentagonal or hexagonal lattice structure (16), which is distinct from the quasi-1D, periodic, ladderlike structure that we observed in the axons of vertebrate brains. Whether the difference is due to invertebrate versus vertebrate animals or peripheral versus central nervous systems is a topic for future investigations.

The periodic, actin-spectrin–based cytoskeleton observed here may not be involved in myosin-dependent axonal transport. If the analogy to the erythrocyte membrane cytoskeleton holds, the capped short actin filaments in the ringlike actin structures in axons are probably bound by tropomyosin (9, 10), which could potentially prevent the binding of myosins. Myosin-dependent axonal transport could, however, be mediated by the long actin filaments that run along the axon shaft. The quasi-1D, periodic, actin-spectrin cytoskeleton may instead provide elastic and stable mechanical support for the axon membrane, given the flexibility of spectrin. Elastic and stable support is particularly important for axons, because they can be extremely long and thin and have to withstand mechanical strains as animals move (37). Indeed, the loss of β-spectrin in *Caenorhabditis elegans* leads to spontaneous breaking of axons, which is caused by mechanical strains generated by animal movement and can be prevented by paralyzing the animal (37). The highly periodical submembrane cytoskeleton can also influence the molecular organization of the plasma membrane by organizing important membrane proteins along the axon. We found that sodium channels were distributed periodically along the axon initial segment in a coordinated manner with the underlying actin-spectrin cytoskeleton. An axonal plasma membrane with periodically varying biochemical and mechanical properties may not only influence how an action potential is generated and propagated, but might also affect how axons interact with other cells.

References and Notes

1. T. D. Pollard, J. A. Cooper, *Science* **326**, 1208 (2009).
2. E. W. Dent, F. B. Gertler, *Neuron* **40**, 209 (2003).
3. L. A. Cingolani, Y. Goda, *Nat. Rev. Neurosci.* **9**, 344 (2008).
4. L. C. Kapitein, C. C. Hoogenraad, *Mol. Cell. Neurosci.* **46**, 9 (2011).
5. A. K. Lewis, P. C. Bridgman, *J. Cell Biol.* **119**, 1219 (1992).
6. F. Korobova, T. Svitkina, *Mol. Biol. Cell* **21**, 165 (2010).
7. N. Hirokawa, *J. Cell Biol.* **94**, 129 (1982).
8. B. J. Schnapp, T. S. Reese, *J. Cell Biol.* **94**, 667 (1982).
9. V. Bennett, A. J. Baines, *Physiol. Rev.* **81**, 1353 (2001).
10. A. J. Baines, *Protoplasma* **244**, 99 (2010).
11. T. J. Byers, D. Branton, *Proc. Natl. Acad. Sci. U.S.A.* **82**, 6153 (1985).
12. S. C. Liu, L. H. Derick, J. Palek, *J. Cell Biol.* **104**, 527 (1987).
13. J. Levine, M. Willard, *J. Cell Biol.* **90**, 631 (1981).
14. V. Bennett, J. Davis, W. E. Fowler, *Nature* **299**, 126 (1982).
15. M. N. Rasband, *Nat. Rev. Neurosci.* **11**, 552 (2010).
16. J. Pielage *et al.*, *Neuron* **58**, 195 (2008).
17. S. W. Hell, *Nat. Methods* **6**, 24 (2009).
18. B. Huang, H. Babcock, X. Zhuang, *Cell* **143**, 1047 (2010).
19. V. Tatavarty, E. J. Kim, V. Rodionov, J. Yu, *PLoS ONE* **4**, e7724 (2009).
20. N. A. Frost, H. Shroff, H. H. Kong, E. Betzig, T. A. Blanpied, *Neuron* **67**, 86 (2010).
21. N. T. Urban, K. I. Willig, S. W. Hell, U. V. Nägerl, *Biophys. J.* **101**, 1277 (2011).
22. I. Izeddin *et al.*, *PLoS ONE* **6**, e15611 (2011).
23. M. J. Rust, M. Bates, X. Zhuang, *Nat. Methods* **3**, 793 (2006).
24. E. Betzig *et al.*, *Science* **313**, 1642 (2006).
25. S. T. Hess, T. P. K. Girirajan, M. D. Mason, *Biophys. J.* **91**, 4258 (2006).
26. M. Bates, B. Huang, G. T. Dempsey, X. Zhuang, *Science* **317**, 1749 (2007).
27. B. Huang, W. Wang, M. Bates, X. Zhuang, *Science* **319**, 810 (2008).
28. Supplementary materials, including materials and methods, are available on *Science* Online.
29. K. Xu, H. P. Babcock, X. Zhuang, *Nat. Methods* **9**, 185 (2012).
30. A. Egner *et al.*, *Biophys. J.* **93**, 3285 (2007).
31. M. R. Galiano *et al.*, *Cell* **149**, 1125 (2012).
32. S. Berghs *et al.*, *J. Cell Biol.* **151**, 985 (2000).
33. M. H. Kole, G. J. Stuart, *Neuron* **73**, 235 (2012).
34. E. Kordeli, S. Lambert, V. Bennett, *J. Biol. Chem.* **270**, 2352 (1995).
35. D. X. Zhou *et al.*, *J. Cell Biol.* **143**, 1295 (1998).
36. A. Brachet *et al.*, *J. Cell Biol.* **191**, 383 (2010).
37. M. Hammarlund, E. M. Jorgensen, M. J. Bastiani, *J. Cell Biol.* **176**, 269 (2007).

Comparative Analysis of Bat Genomes Provides Insight into the Evolution of Flight and Immunity

Guojie Zhang,[1,2]*† Christopher Cowled,[3]* Zhengli Shi,[4]* Zhiyong Huang,[1]* Kimberly A. Bishop-Lilly,[5]* Xiaodong Fang,[1] James W. Wynne,[3] Zhiqiang Xiong,[1] Michelle L. Baker,[3] Wei Zhao,[1] Mary Tachedjian,[3] Yabing Zhu,[1] Peng Zhou,[3,4] Xuanting Jiang,[1] Justin Ng,[3] Lan Yang,[1] Lijun Wu,[4] Jin Xiao,[1] Yue Feng,[1] Yuanxin Chen,[1] Xiaoqing Sun,[1] Yong Zhang,[1] Glenn A. Marsh,[3] Gary Crameri,[3] Christopher C. Broder,[6] Kenneth G. Frey,[5] Lin-Fa Wang,[3,7]† Jun Wang[1,8,9]†

Bats are the only mammals capable of sustained flight and are notorious reservoir hosts for some of the world's most highly pathogenic viruses, including Nipah, Hendra, Ebola, and severe acute respiratory syndrome (SARS). To identify genetic changes associated with the development of bat-specific traits, we performed whole-genome sequencing and comparative analyses of two distantly related species, fruit bat *Pteropus alecto* and insectivorous bat *Myotis davidii*. We discovered an unexpected concentration of positively selected genes in the DNA damage checkpoint and nuclear factor κB pathways that may be related to the origin of flight, as well as expansion and contraction of important gene families. Comparison of bat genomes with other mammalian species has provided new insights into bat biology and evolution.

Bats belong to the order Chiroptera within the mammalian clade Laurasiatheria (1). Although consensus has not been reached on the exact arrangement of groups within Laurasiatheria, a recent study placed Chiroptera as a sister taxon to Cetartiodactyla (whales + even-toed ungulates such as cattle, sheep, and pigs) (2). The Black flying fox (*Pteropus alecto*) and David's Myotis (*Myotis davidii*) represent the Yinpterochiroptera and Yangochiroptera subor-

ders, respectively, and display a diverse range of phenotypes (Fig. 1). Captive colonies, immortalized cell lines, and bat-specific reagents have been developed for these two species; however, genomic data are currently unavailable.

The most conspicuous feature of bats, distinguishing them from all other mammalian species, is the capacity for sustained flight. Positive selection in the oxidative phosphorylation (OXPHOS) pathway suggests that increased metabolic capac-

ity played a key role in its evolution (3), yet the by-products of oxidative metabolism [such as reactive oxygen species (ROS)] can produce harmful side effects including DNA damage (4). We hypothesize that genetic changes during the evolution of flight in bats likely included adaptations to limit collateral damage caused by by-products of elevated metabolic rate. Another phenomenon that has sparked intense interest in recent years is the discovery that bats maintain and disseminate numerous deadly viruses (5). In this context, we further hypothesize that the long-term coexistence of bats and viruses must have imposed strong selective pressures on the bat genome, and the genes most likely to reflect this are those directly related to the first line of antiviral defense—the innate immune system.

We performed high-throughput whole-genome sequencing of individual wild-caught specimens of *P. alecto* and *M. davidii* using the Illumina HiSeq platform (6). More than 100 × coverage high-quality reads were obtained for *P. alecto* and *M. davidii*, which resulted in high-quality assemblies (tables S1 to S3 and fig. S1). The two bat genomes, at ~2 Gb, were smaller in size than other mammals (7) (fig. S2), whereas the number of genes we identified was similar to those of other mammals (21,392 and 21,705 in *P. alecto* and *M. davidii*, respectively) (fig. S3). Both species displayed a high degree of heterozygosity at the whole-genome level (0.45% and 0.28% in *P. alecto* and *M. davidii*, respectively) (tables S4 and S5), whereas repetitive content accounted for slightly less than one-third of each genome (tables S6 and S7). We identified a novel endogenous viral element derived from *Saimiriine herpesvirus 2* that has expanded to 126 copies in *P. alecto* (table S8 and fig. S4). Gene family expansion and contraction analysis (tables S9 to S12) revealed significant expansion ($P < 0.05$) of 71 gene families in *M. davidii* compared with only 13 in *P. alecto*, which may be related to a recent wave of DNA transposon activity (8).

We screened all nuclear-encoded bat genes to identify those for which a single orthologous copy was unambiguously present in both bat species

[1]BGI-Shenzhen, Shenzhen, 518083, China. [2]Centre for Social Evolution, Department of Biology, University of Copenhagen, Universitetsparken 15, DK-2100 Copenhagen, Denmark. [3]Commonwealth Scientific and Industrial Research Organization (CSIRO) Australian Animal Health Laboratory, Geelong, Victoria 3220, Australia. [4]State Key Laboratory of Virology, Wuhan Institute of Virology, Chinese Academy of Sciences, Wuhan 430071, China. [5]Naval Medical Research Center and Henry M. Jackson Foundation, Fort Detrick, Frederick, MD 21702, USA. [6]Department of Microbiology and Immunology, Uniformed Services University of the Health Sciences, Bethesda, MD 20814, USA. [7]Program in Emerging Infectious Diseases, Duke–National University of Singapore Graduate Medical School, Singapore 169857. [8]Novo Nordisk Foundation Center for Basic Metabolic Research, University of Copenhagen, DK-2200 Copenhagen, Denmark. [9]Department of Biology, University of Copenhagen, DK-2200 Copenhagen, Denmark.

*These authors contributed equally to this work.
†To whom correspondence should be addressed. E-mail: zhanggj@genomics.org.cn (G.Z.); linfa.wang@csiro.au (L.-F.W.); wangj@genomics.org.cn (J.W.)

Fig. 1. Comparison of bat biological traits. *P. alecto* and *M. davidii* represent two distinct Chiropteran suborders and demonstrate diverse evolutionary adaptations. PNG, Papua New Guinea.
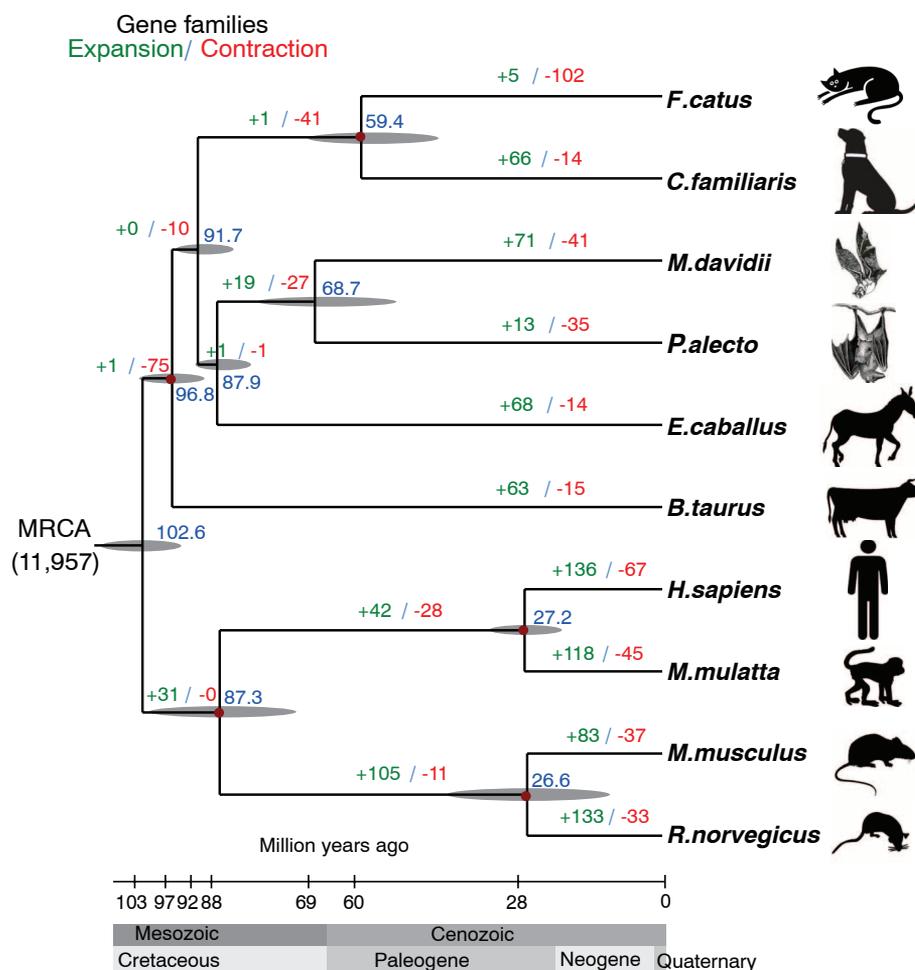
Trait	*Myotis davidii*	*Pteropus alecto*
Common name	David's Myotis	Black flying fox
Suborder	Yangochiroptera	Yinpterochiroptera
Distribution	China	Australia, PNG, Indonesia
Habitat	Rock cavities	Trees, mangroves, rainforest
Diet	Insectivorous	Frugivorous, nectarivorous
Hibernation	Hibernates Nov-May	No
Echolocation	Yes	No
Viral reservoir	Potential	Yes

Fig. 2. Phylogenomic analysis. Maximum-likelihood phylogenomic analysis of 2492 genes from *M. davidii*, *P. alecto*, and eight mammalian species. Divergence time estimates in blue, gene family expansion events in green, and gene family contraction events in red. MRCA, most recent common ancestor.

as well as in human, rhesus macaque, mouse, rat, dog, cat, cattle, and horse. From this, 2492 genes were used to perform maximum-likelihood and Bayesian phylogenomic analysis (Fig. 2 and figs. S5 to S7). All phylogenetically informative signals, including concatenated nucleotides and amino acids, vigorously supported bats as a member of Pegasoferae (Chiroptera + Perissodactyla + Carnivora) (*9*), with the bat lineage diverging from the *Equus* (horse) lineage ~88 million years ago, buttressed by findings at the transcript level (*10*). However, phylogenetic reconstruction with mitochondrial DNA sequences resulted in bats occupying an outlying position in Laurasiatheria (fig. S8). The incongruence between nuclear and mitochondrial trees likely reflects rapid evolution of the mitochondrial genome of the bat ancestor during the evolution of flight (*3*).

To identify mechanisms that facilitated the origin of flight in bats, we surveyed genes involved in detection and repair of genetic damage. A high proportion of genes in the DNA damage checkpoint–DNA repair pathway were found to be under positive selection in the bat ancestor, including *ATM*, the catalytic subunit of DNA-dependent protein kinase (DNA-PKc), *RAD50*, *KU80*, and *MDM2* (Fig. 3A and Table 1). We propose that these changes may be directly related to minimizing and/or repairing the negative effects of ROS generated as a consequence of flight. Additionally in this pathway, *TP53* (*p53*) and *BRCA2* were shown to be under positive selection in *M. davidii*, whereas *LIG4* was under positive selection in *P. alecto* (Table 1). Bat-specific mutations in a nuclear localization signal in *p53* and a nuclear export signal in *MDM2* (Fig. 3B and fig. S9) may affect subcellular localization and function in both species (*11*, *12*). Other candidate flight-related genes under positive selection in the bat ancestor included *COL3A1*, involved in skin elasticity, and *CACNA2D1*, which has a role in muscle contraction (table S13).

We next examined genes of the innate immune system (Table 1). Positively selected genes in the bat ancestor included c-*REL*, a member of the nuclear factor κB (NF-κB) family of transcription factors, which also contained amino acid changes potentially affecting inhibitor of NF-κB (IκB) binding (fig. S10). In addition to diverse roles in innate and adaptive immunity (*13*), c-*REL* plays a role in the DNA damage response by activating *ATM* (*14*) and *CLSPN* (*15*), whereas *ATM* is also an upstream regulator of *NF-κB* (*16*). The DNA damage response plays an important role in host defense and is a known target for virus interaction (*17*), which raises the possibility that changes in DNA damage response mechanisms during selection for flight could have influenced the bat immune system.

It is intriguing that both *P. alecto* and *M. davidii* have lost the entire locus containing the PYHIN gene family, including *AIM2* and *IFI16*, both of which are involved in sensing microbial DNA and the formation of inflammasomes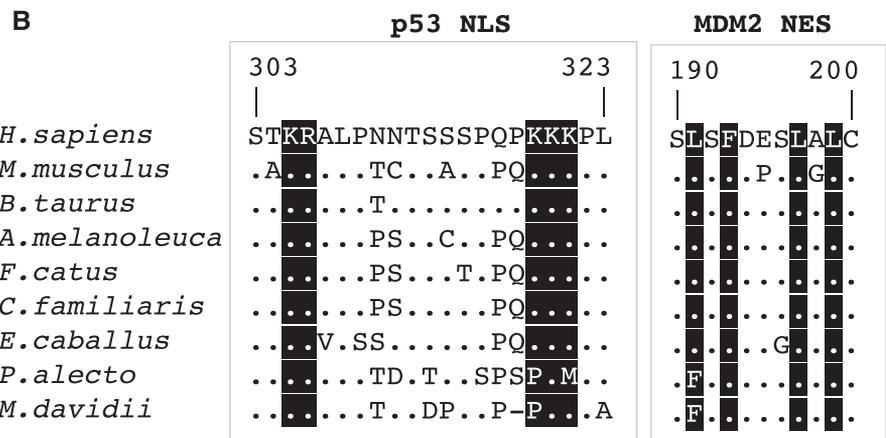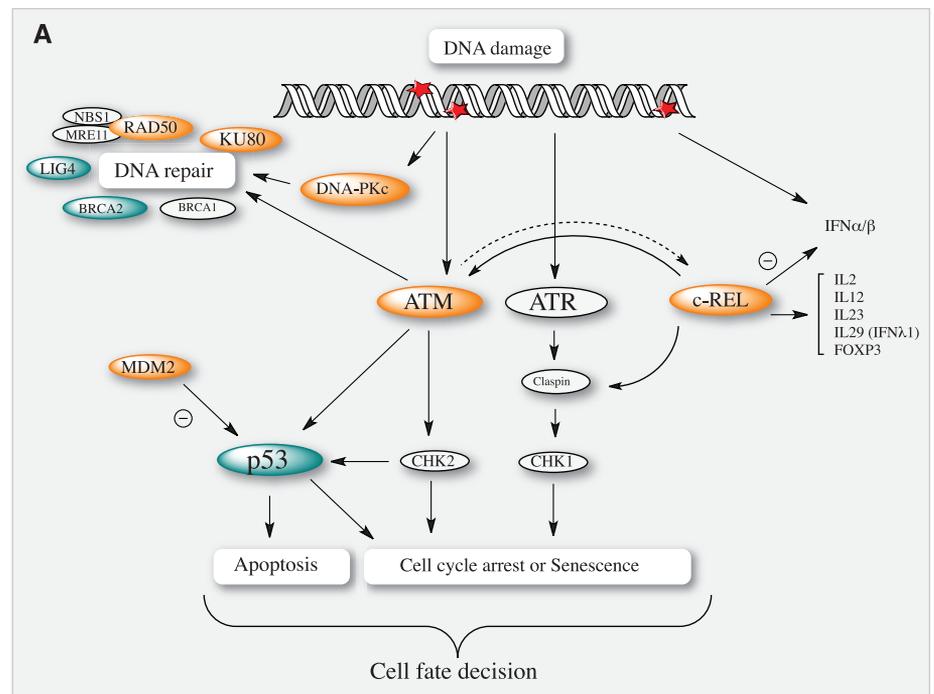 (fig. S11). The association between PYHIN genes and cell cycle regulation in other species (*18*) hints that loss of the PYHIN family in bats may be connected to changes in the DNA damage pathway, because at least one PYHIN gene is present in all other major groups of eutherian mammals (*19*). *NLRP3*, triggered by both viral infection and ROS in other mammals (*20*), plays an analogous role to *AIM2* in inflammasome assembly and was also under positive selection in the bat ancestor (Table 1).

Natural killer (NK) cells provide a first line of defense against viruses and tumors and include two families of NK cell receptors; killer-cell immunoglobulin like receptors (KIRs), encoded by genes in the leukocyte receptor complex (LRC), and killer cell lectin-like receptors (KLRs, also known as Ly49 receptors), encoded within the natural killer gene complex (NKC). KLRs and KIRs were entirely absent in *P. alecto* and reduced to a single *Ly49* pseudogene in *M. davidii* (table S14). KIR-like receptors identified in other species (*21*) were also absent from both *P. alecto* and *M. davidii* genomes, which was supported by transcript analysis in *P. alecto* (*10*). This likely indicates that bat NK cells use a novel class of receptors to recognize classical major histocompatibility complex class I molecules. Furthermore, additional LRC members of the immunoglobulin superfamily [including sialic acid–binding immunoglobulin-like lectins (SIGLECs), leukocyte

Fig. 3. Accelerated evolution in the DNA damage checkpoint in bats. (**A**) Positive selection in the DNA damage checkpoint–DNA repair pathway. Genes under positive selection in the bat ancestor are highlighted in orange. Genes under positive selection in *M. davidii* only (*p53*, *BRCA2*) or *P. alecto* only (*LIG4*) are highlighted in blue. IFN, interferon; IL, interleukin. (**B**) Mutations unique to bats were detected in the functionally relevant regions of the *p53* nuclear localization signal (NLS) and *MDM2* nuclear export signal (NES) (black shading).

Table 1. DNA damage checkpoint and innate immune genes under positive selection in the bat lineages. The rate ratio ω of dN/dS was calculated using multiprotein alignments of *P. alecto* and *M. davidii* sequences with orthologous sequences from human, rhesus macaque, mouse, rat, dog, cattle, and horse. $\omega0$ is the average ratio in all branches, $\omega1$ is the average ratio in nonbat branches, and $\omega2$ is the ratio in the bat branch. A low *P* value indicates that the $\omega2$ model fits the data better than the $\omega1$ model.

Lineage	Symbol	Gene	$\omega0$ (average)	$\omega1$ (other)	$\omega2$ (target)	*P* value
Ancestor	TLR7	Toll-like receptor 7	0.2821	0.2670	2.7778	3.54E-07
	ATM	Ataxia telangiectasia mutated	0.20096	0.19595	0.7163	1.34E-05
	MDM2	Mdm2 p53 binding protein homolog (mouse)	0.13358	0.12615	0.81085	4.05E-04
	NLRP3	NLR family, pyrin domain–containing 3	0.1788	0.1714	1.1884	1.93E-04
	MAP3K7	Mitogen-activated protein kinase kinase kinase 7	0.0216	0.0194	0.4786	8.93E-03
	RAD50	RAD50 homolog	0.09657	0.09343	0.28882	7.95E-03
	PRKDC	Protein kinase, DNA-activated, catalytic polypeptide	0.23036	0.22768	0.45155	6.80E-03
	KU80	X-ray repair complementing defective repair in Chinese hamster cells 5	0.31145	0.30436	0.91747	3.75E-02
	c-REL	v-rel reticuloendotheliosis viral oncogene homolog (avian)	0.2495	0.2403	1.5717	1.11E-02
P. alecto	TBK1	TANK-binding kinase 1	0.0643	0.0522	0.2930	1.29E-09
	LIG4	Ligase IV, DNA, ATP-dependent	0.12033	0.11376	0.24797	8.91E-04
	IL18	Interleukin 18 (interferon-γ–inducing factor)	0.5298	0.4532	1.7647	2.66E-04
	IFNG	Interferon-γ	0.5010	0.4527	1.3282	4.89E-03
	ISG15	ISG15 ubiquitin-like modifier	0.2069	0.1909	0.4387	2.63E-02
	DDX58	DEAD (Asp-Glu-Ala-Asp) box polypeptide 58	0.3040	0.2923	0.4661	1.23E-02
M. davidii	IFNAR1	Interferon (α, β, and ω) receptor 1	0.4954	0.4723	31.0924	7.00E-03
	TP53	Tumor protein p53	0.25623	0.23933	0.48123	7.00E-03
	BRCA2	Breast cancer 2, early onset	0.49002	0.47732	0.64213	1.31E-03
	IRAK4	Interleukin-1 receptor–associated kinase 4	0.1670	0.1583	0.3531	1.96E-02

immunoglobulin-like receptors (LILRs), carcino-embryonic antigen-related cell adhesion molecules (CEACAMs), and leukocyte-associated immunoglobulin-like receptors (LAIRs)] have undergone considerable gene duplication in *M. davidii* and other mammals yet have almost completely failed to expand in *P. alecto* (fig. S12). As the genes encoded within the LRC bind a variety of ligands and play multiple roles in immune regulation, these observations have diverse implications for differences in immune function between *P. alecto* and *M. davidii* and between bats and other mammals.

We identified seven complete and two partial copies of the digestive enzyme *RNASE4* in *M. davidii* (table S15), whereas *P. alecto RNASE4* has acquired a frameshift mutation resulting in loss of catalytic residues (fig. S13). We also identified critical amino acid changes in *M. davidii RNASE4* genes (relative to the mammalian consensus) that suggest diversification of substrate specificity (fig. S13). With a proven role in host defense against RNA viruses (*22*), *RNASE4* expansion in *M. davidii* may have implications for virus resistance but may also reflect the insectivorous diet of *M. davidii*, in contrast with that of *P. alecto*, which consumes predominantly fruit, flowers, and nectar.

M. davidii also differs from *P. alecto* in aspects including hibernation and echolocation (Fig. 1). Bile salt–stimulated lipase (BSSL), capable of hydrolyzing triglycerides into monoglycerides and subsequently releasing digestible free fatty acids, has been specifically expanded in *M. davidii* compared with *P. alecto* and other mammals (fig. S14). In addition, we observed six candidate genes related to hibernation, which showed positive se-

lection in *M. davidii* and three other hibernating species relative to nonhibernators (table S16). Seven echolocation-related genes, including new candidates *WNT8A* and *FOS* (a subunit of the AP-1 transcription factor), had significantly higher ratio of nonsynonymous to synonymous substitutions (dN/dS) in the echolocating *M. davidii* branch relative to non-echolocating branches (table S17). Of note, the third exon in *M. davidii FOXP2* had even greater variation from the mammalian consensus than two previously identified variable sites (fig. S15), which suggests a specific transcript variant is involved in echolocation (*23*).

In summary, comparative analysis of *P. alecto* and *M. davidii* genomes has provided insight into the phylogenetic placement of bats and has revealed evidence of genetic changes that may have contributed to their evolution. Gene duplication events played a particularly prominent role in the evolution of *Myotis* bats and may have helped contribute to their speciation. Concentration of positively selected genes in the DNA damage checkpoint pathway in bats may indicate an important step in the evolution of flight, whereas evidence of change in components shared by the DNA damage pathway and the innate immune system raises the interesting possibility that flight-induced adaptations have had inadvertent effects on bat immune function and possibly also life expectancy (*24*). The data generated by this study will help to address major gaps in our understanding of bat biology and to provide new directions for future research.

References and Notes
1. E. C. Teeling *et al.*, *Science* **307**, 580 (2005).
2. M. F. Nery, D. J. González, F. G. Hoffmann, J. C. Opazo, *Mol. Phylogenet. Evol.* **64**, 685 (2012).
3. Y. Y. Shen *et al.*, *Proc. Natl. Acad. Sci. U.S.A.* **107**, 8666 (2010).
4. A. Barzilai, G. Rotman, Y. Shiloh, *DNA Repair (Amsterdam)* **1**, 3 (2002).
5. L. F. Wang, P. J. Walker, L. L. Poon, *Curr. Opin. Virol.* **1**, 649 (2011).
6. Materials and methods are available as supplementary materials on *Science* Online.
7. J. D. L. Smith, T. R. Gregory, *Biol. Lett.* **5**, 347 (2009).
8. E. J. Pritham, C. Feschotte, *Proc. Natl. Acad. Sci. U.S.A.* **104**, 1895 (2007).
9. H. Nishihara, M. Hasegawa, N. Okada, *Proc. Natl. Acad. Sci. U.S.A.* **103**, 9929 (2006).
10. A. T. Papenfuss *et al.*, *BMC Genomics* **13**, 261 (2012).
11. K. O'Keefe, H. P. Li, Y. P. Zhang, *Mol. Cell. Biol.* **23**, 6396 (2003).
12. J. Roth, M. Dobbelstein, D. A. Freedman, T. Shenk, A. J. Levine, *EMBO J.* **17**, 554 (1998).
13. T. D. Gilmore, S. Gerondakis, *Genes Cancer* **2**, 695 (2011).
14. A. De Siervi *et al.*, *Cell Cycle* **8**, 2093 (2009).
15. N. S. Kenneth, S. Mudie, S. Rocha, *EMBO J.* **29**, 2966 (2010).
16. K. Brzóska, I. Szumiel, *Mutagenesis* **24**, 1 (2009).
17. A. S. Turnell, R. J. Grand, *J. Gen. Virol.* **93**, 2076 (2012).
18. S. A. Schattgen, K. A. Fitzgerald, *Immunol. Rev.* **243**, 109 (2011).
19. J. A. Cridland *et al.*, *BMC Evol. Biol.* **12**, 140 (2012).
20. J. Tschopp, K. Schroder, *Nat. Rev. Immunol.* **10**, 210 (2010).
21. J. G. Sambrook, S. Beck, *Curr. Opin. Immunol.* **19**, 553 (2007).
22. F. Cocchi *et al.*, *Proc. Natl. Acad. Sci. U.S.A.* **109**, 5411 (2012).
23. G. Li, J. H. Wang, S. J. Rossiter, G. Jones, S. Y. Zhang, *PLoS ONE* **2**, e900 (2007).
24. A. K. Brunet-Rossinni, S. N. Austad, *Biogerontology* **5**, 211 (2004).

Tunable Signal Processing Through Modular Control of Transcription Factor Translocation

Nan Hao,[1,2] Bogdan A. Budnik,[1] Jeremy Gunawardena,[3] Erin K. O'Shea[1,2]*

Signaling pathways can induce different dynamics of transcription factor (TF) activation. We explored how TFs process signaling inputs to generate diverse dynamic responses. The budding yeast general stress–responsive TF Msn2 acted as a tunable signal processor that could track, filter, or integrate signals in an input-dependent manner. This tunable signal processing appears to originate from dual regulation of both nuclear import and export by phosphorylation, as mutants with one form of regulation sustained only one signal-processing function. Versatile signal processing by Msn2 is crucial for generating distinct dynamic responses to different natural stresses. Our findings reveal how complex signal-processing functions are integrated into a single molecule and provide a guide for the design of TFs with "programmable" signal-processing functions.

Many transcription factors (TFs) display diverse activation dynamics in response to various external stimuli (*1–4*). To investigate how TFs process upstream signals, we studied the *Saccharomyces cerevisiae* general stress–responsive TF Msn2 (*5*). In the absence of stress, Msn2 is phosphorylated by protein kinase A (PKA) and localized to the cytoplasm; in response to stress, Msn2 is dephosphorylated and translocates to the nucleus, where it induces gene expression (*5*).

Natural stresses elicit highly variable dynamics of Msn2 nuclear translocation (Fig. 1A) (*6, 7*), which are thought to result from oscillatory signaling inputs (presumably PKA activity) (*8*). To study how Msn2 processes oscillatory PKA inputs, we used an engineered yeast strain (*6*) carrying mutations in all three PKA isoforms that enable selective inhibition of PKA activity by a cell-permeable inhibitor, 1-NM-PP1 (*9*). We used this synthetic system and a microfluidics plat-

form (*10*) mounted on a microscope to produce oscillatory inputs of PKA inhibition and monitored translocation of Msn2 to the nucleus. The

input amplitude was chosen on the basis of the steady-state amount of Msn2 nuclear localization in response to sustained inputs: high-amplitude input (3 μM 1-NM-PP1) led to maximal nuclear localization of Msn2, whereas low-amplitude input (0.2 μM 1-NM-PP1) induced an intermediate amount of nuclear localization (Fig. 1B, black circles). The pulse duration of oscillatory input was selected on the basis of duration of pulsatile Msn2 nuclear bursts in the physiological response to glucose limitation (*6*). With high-amplitude oscillatory input, each input pulse induced a large amount of nuclear localization (Fig. 1C, left). In contrast, oscillatory input with low amplitude barely elicited any localization responses, although sustained input with the same amplitude led to a half-maximal amount of nuclear localization (Fig. 1C, right). Therefore, Msn2 filters temporal fluctuations of the input in an amplitude-dependent manner such that it tracks high-amplitude inputs, but responds in a limited manner to low-amplitude signals.
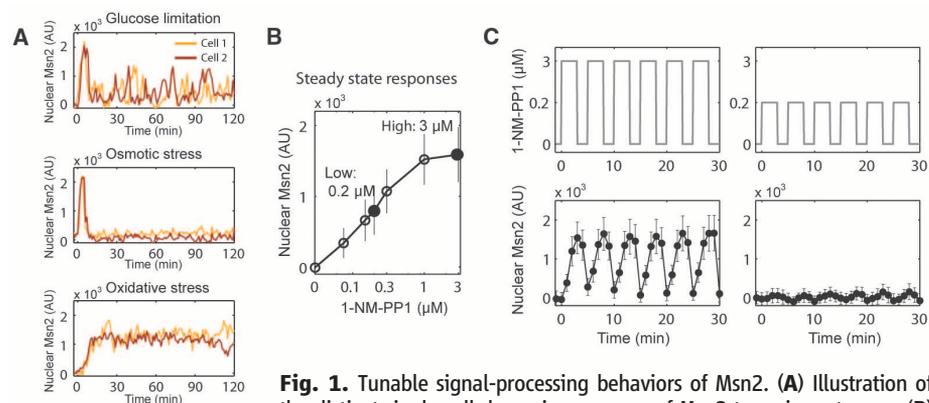

Fig. 1. Tunable signal-processing behaviors of Msn2. (**A**) Illustration of the distinct single-cell dynamic responses of Msn2 to various stresses. (**B**) Steady-state abundance of Msn2 in the nucleus in response to various concentrations of 1-NM-PP1. In response to each concentration of 1-NM-PP1, Msn2 exhibited uniform and stable nuclear localization in single cells and did not exhibit stochastic fluctuations as observed in natural stress responses. Open circles: responses to different concentrations of 1-NM-PP1; closed circles: responses to 3 μM and 0.2 μM 1-NM-PP1, which are used as high- and low-amplitude inputs, respectively, for the following analyses. AU, arbitrary unit. (**C**) Averaged single-cell time traces of Msn2 nuclear translocation (bottom: $n \approx 50$ cells; error bar: single-cell variances) in response to oscillatory inputs with high and low amplitudes (top). (Left) High-amplitude input produced by 3 μM 1-NM-PP1; (right) low-amplitude input produced by 0.2 μM 1-NM-PP1. Pulse duration of 3 min; pulse interval of 2 min. To emphasize the fact that 3 μM 1-NM-PP1 elicits a steady-state response that is about twice the response elicited by 0.2 μM 1-NM-PP1, the top *y* axes are not presented on a linear scale.

[1]Harvard University Faculty of Arts and Sciences Center for Systems Biology, Cambridge, MA 02138, USA. [2]Howard Hughes Medical Institute, Department of Molecular and Cellular Biology, and Department of Chemistry and Chemical Biology, Harvard University, Cambridge, MA 02138, USA. [3]Department of Systems Biology, Harvard Medical School, Boston, MA 02115, USA.

*To whom correspondence should be addressed. E-mail: erin_oshea@harvard.edu